An integrated SEM–Newmark model for physics-based regional coseismic landslide assessment

Article *in* Soil Dynamics and Earthquake Engineering · February 2020

DOI: 10.1016/j.soildyn.2020.106066

6 authors, including:

Duruo Huang
Tsinghua University
44 PUBLICATIONS **251** CITATIONS
SEE PROFILE

Gang Wang
The Hong Kong University of Science and Technology
79 PUBLICATIONS **1,023** CITATIONS
SEE PROFILE

Feng Jin
Tsinghua University
205 PUBLICATIONS **1,606** CITATIONS
SEE PROFILE

Kewei Feng
The Hong Kong University of Science and Technology
1 PUBLICATION **0** CITATIONS
SEE PROFILE

Soil Dynamics and Earthquake Engineering 132 (2020) 106066

Contents lists available at ScienceDirect

Soil Dynamics and Earthquake Engineering

journal homepage: http://www.elsevier.com/locate/soildyn

An integrated SEM-Newmark model for physics-based regional coseismic landslide assessment

Duruo Huang [a], Gang Wang [b,*], Chunyang Du [b], Feng Jin [a], Kewei Feng [b], Zhengwei Chen [b]

[a] Department of Hydraulic Engineering, Tsinghua University, Beijing, China
[b] Department of Civil and Environmental Engineering, The Hong Kong University of Science and Technology, Hong Kong SAR, China

ARTICLE INFO

Keywords:
Coseismic landslide hazard
Spectral element method
Newmark displacement analyses
Topographic amplification
Case studies

ABSTRACT

Earthquake-induced landslides are one of the most catastrophic effects of earthquakes, as evidenced by many historic events over the past decades, such as the 1994 Northridge earthquake in California and the 2008 Wenchuan earthquake in China. Realistic prediction of coseismic landslides is crucial for the design of key infrastructure and to protect human lives in seismically active regions. To date, analytical methods for estimating coseismic landslides have been based on highly simplified models. In this study, an integrated Spectral Element Method (SEM)-Newmark model is developed to directly simulate three-dimensional wave field in complex topography on a regional scale, while the associated landslide is indicated by the Newmark sliding displacement analysis considering key model factors. Topographic amplification, soil response, near-field characteristics of earthquake shaking and hydrogeological conditions can be simulated, and their effects on coseismic landslides are studied. In this paper, two regional-scale case studies were conducted using the developed SEM-Newmark model, including landslide hazard assessment for natural terrain in the western part of Hong Kong island, and the massive landslides occurred during the 2014 **M**6.5 Ludian earthquake in China. These case studies demonstrated that the proposed integrated model can be effectively used for regional-scale coseismic landslide hazard assessment under various earthquake scenarios and hydrogeological conditions.

1. Introduction

Earthquake-induced landslides are one of the most catastrophic effects of earthquakes, as evidenced by many historic events over the past decades. As a few examples, the 1994 Northridge earthquake triggered more than 11,000 landslides [1]. During the 2008 Wenchuan earthquake in China, the earthquake-induced Tangjiashan landslide with over 20.37 million m^3 mass movement blocked the main river channel and formed a landslide dam, putting millions of people downstream at risk [2]. Realistic prediction of coseismic landslides is crucial for the design of key infrastructure and to protect human lives in seismically active regions. Among many existing methods for landslide assessment, the Newmark sliding mass model has been extensively utilized to estimate earthquake-induced displacements in slopes, earth dams and landfills since the 1960s [3–9]. The Newmark displacement has been widely accepted as an index to categorize landslide hazard [3,10]. There have been many empirical relations developed for estimating earthquake-induced sliding displacements based on Newmark-type analyses [3–11]. Yet, coseismic landslides primarily occur close to the earthquake epicenter, where near-fault ground motions have distinctive features including as being strongly polarized and containing a velocity pulse [12–15]. It is well known that seismic motions can be significantly altered by three-dimensional topographic features of natural terrain. Moreover, coupling effect between topography and soil-amplification leads to complex wave propagation patterns due to scattering and diffracting of waves within the low-velocity near-surface layers [16–18]. These ground-motion effects have significant impact on coseismic landslide assessment, but only limited efforts have been devoted to consider these effects in empirical models [19,20]. There is a clear need to develop innovative numerical schemes to address the above challenges.

In this paper, a physics-based model is proposed by coupling Spectral Element Method (SEM) and Newmark displacement method for regional scale analyses of coseismic landslides. The SEM is efficient in modeling a 3D wave field in complex topography on a scale of hundreds of kilometers through physics-based modeling [18,21–23]. As illustrated in Fig. 1, near-field characteristics of earthquake shaking and topographic amplification can be faithfully simulated, and their effects on coseismic

* Corresponding author.
E-mail address: gwang@ust.hk (G. Wang).

https://doi.org/10.1016/j.soildyn.2020.106066
Received 18 June 2019; Received in revised form 22 January 2020; Accepted 24 January 2020

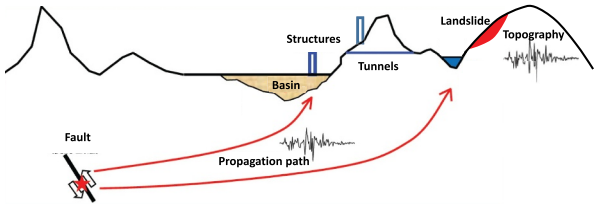

Fig. 1. Illustration of regional-scale simulation of coseismic landslides.

landslides will be studied. Note that SEM is a continuum method that cannot easily capture the mass sliding process of slopes, which usually involves strain localization and generation of slip band. Therefore, coupling the Newmark sliding block analysis with SEM can effectively model the associated landslide with consideration of key hydrogeological properties. The coupled SEM-Newmark method will become a first-of-its-kind numerical tool for assessing coseismic landslides at a regional scale.

Two case studies are conducted using this method to investigate landslide hazard in Hong Kong island, and the Hongshiyan landslide during the 2014 M6.5 Ludian earthquake in China. These two cases demonstrate application of the proposed integrated method in two scenarios: the Hong Kong study emphases on the importance of topographic amplification, soil strata and hydrogeological condition, and the sliding mass is relatively shallow. On the other hand, the Hongshiyan landslide case simulates entire process of fault rupture, wave propagation and landslide over a large domain. This case is featured by deep seated landslides that were triggered by strong near-source motions and topographic effects. These examples demonstrate the importance of topographic amplification, in-situ hydrogeological condition and near-fault effect on coseismic landslides assessments, which has not yet been well understood using empirically-based approaches.

2. An integrated SEM-Newmark method for regional-scale coseismic landslide hazard assessment

2.1. The SEM-Newmark framework

In this study, an integrated SEM-Newmark method is developed for regional-scale coseismic landslide hazard assessment by leveraging physics-based simulation of seismic wave field and topographic amplification of earthquake ground motions. The SEM is a high-order finite element method (FEM) that combines the flexibility of a FEM with the accuracy of a spectral method. It has distinct advantage in modeling large-scale 3D seismic wave propagation because it has diagonal mass matrix and thus can be easily implemented in parallel computing [21–23]. Compared with the commonly used finite element method, the SEM is capable of achieving high accuracy in modeling 3D wave field. For example, if a polynomial degree of 4 is used in interpolation, one element per wavelength in SEM can be very accurate. In other words, if the element size is 10 m and shear wave velocity is 200 m/s, the highest frequency that the SEM can simulate will be up to 20 Hz, which is sufficient to cover the most significant frequency content in earthquake waves. Given these advantages, the SEM has gained interest for problems related to 3D seismic wave propagation in a regional scale with a computational domain up to hundreds of kilometers [18,22]. In this study, the 3D SEM is used to model a large domain of competent rock underlying soils that are susceptible to landslide under earthquake loading.

Fig. 2 illustrates the coupling scheme between SEM and Newmark displacement analysis method. The computational framework primarily includes four steps:

(i) *Develop 3D Spectral Element model using DEM and geological data:* A high-resolution 3D spectral element model is developed based on digital terrain and extensive geological/geotechnical borehole data to construct shear velocity structure of the simulation domain. Fault rupture process can be incorporated to simulate near-source ground motions.

(ii) *Conduct physics-based simulation of wave propagation*: Conduct the spectral element analyses to model the 3D wave field in complex topography. Previous research demonstrated that using equivalent acceleration provides an adequate estimate of seismic loading for sliding mass analyses [24,25]. Therefore, the averaged response acceleration along the soil column is adopted in the current study as the acceleration time history to conduct the Newmark sliding block analyses.

(iii) *Determine the critical acceleration of slopes:* A digital elevation model (DEM) is used to extract elevation data and generate a map of slope angle, aspect direction for sliding, followed by determining soil properties (i.e. cohesion, friction angle, degree of saturation and layer thickness). The landslide will be triggered when ground shaking exceeds the critical acceleration. Determination of the critical acceleration of a slope will be discussed in details in Section 2.2.

(iv) *Conduct Newmark displacement analyses and generate regional landslide hazard map:* The map of slope displacement is generated using computed Newmark sliding displacement. As discussed in Section 2.2, both shallow and deep sliding can be considered using the concept of equivalent accelerations in the Newmark calculation. In the end, a regional landslide hazard map showing Newmark displacement distribution can be generated over the study region.

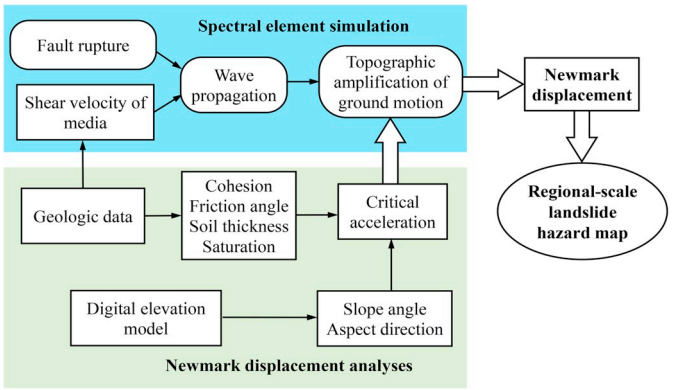

Fig. 2. Flow chart of the integrated method for regional-scale coseismic landslide assessment.

2.2. The Newmark sliding displacement analyses

In this study, the Newmark sliding mass model is adopted to compute coseismic sliding displacement on slopes under earthquake loading. The Newmark model assumes the sliding mass is rigid during earthquakes, while deformation of the mass can be neglected. Sliding occurs on a well-defined infinite slope when acceleration along the slope direction (a_s) exceeds a critical acceleration (a_c), and the block continues to slide until the relative velocity between the block and ground reaches zero. The permanent displacement of sliding block, also referred to the Newmark displacement, is computed by integrating the velocity time history. Although no slope virtually perfectly satisfies the assumption of infinite slope model, many natural landslides are predominantly plane failure along relatively shallow soil-rock interface. The idealization therefore provides a useful approximation that can help to identify the landslide hazard at the reconnaissance stage.

Conventional Newmark analysis only considers ground shaking a_s along the slope direction (see Fig. 3(a)). The critical acceleration is a simple function of the static factor of safety (*FS*) and the slope angle α:

$$a_c = (FS - 1)g \sin \alpha \quad (1)$$

According to Ref. [26], the static factor of safety is computed using a limit-equilibrium model of an infinite slope:

$$FS = \frac{c'}{\gamma_t t \sin \alpha} + \frac{\tan \varphi'}{\tan \alpha} - \frac{m\gamma_w \tan \varphi'}{\gamma_t \tan \alpha} \quad (2)$$

where φ' is the effective friction angle of the soil, c' is the effective cohesion, α is the slope angle, γ_t is the total unit weight of the soil, γ_w is the unit weight of water and t is the thickness of the sliding block in normal direction and m is the proportion of soil that is submerged. The above equation is applicable for slip surface below the water table. For an unsaturated soil slope, the matric suction increases shear resistance along the slip surface. The static factor of safety can be modified as [27]:

$$FS = \frac{c' + (\sigma_n - u_a)\tan \varphi' + (u_a - u_w)\tan \varphi^b}{\gamma_t t \sin \alpha} \quad (3)$$

where u_a is the pore air pressure, u_w is the pore water pressure, (u_a-u_w) is the matric suction, σ_n is the total normal stress, σ_n - u_a is the net normal stress on the slip surface and φ^b is an angle indicating the rate of increase in shear strength related to matric suction. According to GEO report [28], for soils with low degree of saturation, φ^b is approximately equal to the value of φ'. Then Eq. (3) can be expressed as:

$$FS = \frac{c' - \psi \tan \varphi'}{\gamma_t t \sin \alpha} + \frac{\tan \varphi'}{\tan \alpha} \quad (4)$$

where ψ is the matric suction (a negative value). Note that in the above expression, the matric suction serves as a part of apparent cohesion, and it could significantly affect evaluation of the sliding resistance. Combining Eq. (1) and Eq. (4), we can obtain the following equation for critical acceleration, which is a constant value:

$$a_{c,constant} = g \tan \varphi' \cos \alpha + \frac{c' g - \psi g \tan \varphi'}{\gamma_t t} - g \sin \alpha \quad (5)$$

Note that the above equation applies when the soil slope is unsaturated and ground acceleration is only along the slope direction. However, ground motions are three dimensional, as illustrated in Fig. 3(b). Acceleration normal to the slope dip direction, $a_n(t) = a_v(t)\cos \alpha + a_h(t)\sin \alpha$, should be considered to determine the yield acceleration as:

$$a_{c,transient}(t) = \tan \varphi' (g \cos \alpha - a_v(t)\cos \alpha - a_h(t)\sin \alpha) + \frac{c' g - \psi g \tan \varphi'}{\gamma_t t} - g \sin \alpha \quad (6)$$

where a_h (t), a_v (t) are horizontal and vertical accelerations on the sliding mass. Note that the acceleration that drives the sliding block down the slope takes into account of both horizontal and vertical accelerations, i.e., $a_s(t) = a_h(t)\cos \alpha - a_v(t)\sin \alpha$. Newmark sliding will be triggered once

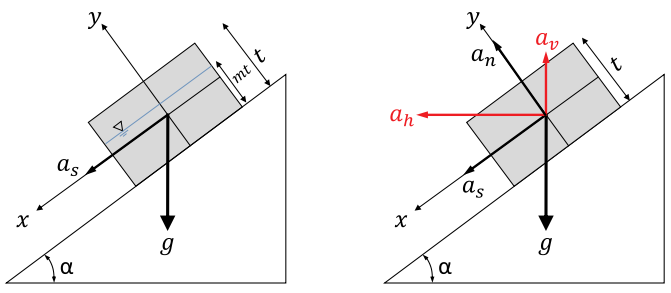

Fig. 3. The Newmark sliding block model (a) only considering acceleration along the sliding direction, (b) considering acceleration along and normal to the sliding direction.

$a_s(t)$ exceeds the transient critical acceleration $a_{c,transient}(t)$. Note that the matric suction ψ is included in determining the yield acceleration in Eq. (6) if soil is partially saturated. When the sliding plane is submerged, the ψ term (a negative value) is simply replaced by the pore pressure determined by $m\gamma_w t$ (a positive value), where m is the proportion of soil that is submerged (Fig. 3(a)), showing the location of groundwater table.

Note that the Newmark model assumes the sliding block is rigid, and it is most suitable for shallow sliding. For deep seated landslide, the sliding masses are flexible and respond to the earthquake loading dynamically. Therefore, the concept of "equivalent acceleration" [11] shall be used in the Newmark displacement calculation via Eq. (5) or (6). At each location, the equivalent accelerations, $\overline{a}_h$ (t) and $\overline{a}_v$ (t), are calculated by SEM as the accelerations averaged along the vertical profile of the sliding mass, which are also equivalent to the forces acting along the sliding plane. Therefore, the SEM-Newmark model is essentially a decoupled approach that can be used for both shallow and deep-seated sliding. Dynamic response analysis of the sliding mass is calculated by SEM by assuming that no slip occurs along the failure plane, then the rigid Newmark sliding block calculation is performed using the equivalent acceleration-time histories. The concept can be equally applied to shallow and deep-seated sliding, although for shallow sliding, accelerations at the ground surface can be simply used.

The integrated SEM-Newmark model provides a viable approach to directly simulate coseismic landslides considering wave propagation, complex topography and hydrogeological conditions. In the following sections, two case studies are carried out, including coseismic landslide assessment of natural terrain landslide in the western part of the Hong Kong Island, and the massive landslide case history during the 2014 M6.5 Ludian earthquake in Yunnan province, China. These two cases are selected because the former represents slope failure in relatively shallow soils considering topographic amplification and in-situ hydrogeological condition, while the latter is featured by landslides triggered by near-source strong-directivity motions.

3. Coseismic landslide assessment for Hong Kong island

3.1. Geological setting and model setup

Hong Kong is a mountainous region with many buildings and infrastructures built on slopes and mountain tops due to paucity of land. The Hong Kong Island, the heart of the city, is densely populated with 1.3 million people. In the past, numerous landslides have occurred in the area due to heavy rainfall [29]. Historically, Hong Kong is considered as a low-to-moderate seismicity region based on historical data, and observation over the past 100 years have seen no severe seismic damage [30]. However, the risk of earthquakes and associated landslides cannot be neglected considering a large population living by the hillside and on the hill slopes. To date, earthquake-induced landslide assessment for this region has not yet been thoroughly conducted. Recent PSHA study indicated that the peak ground acceleration is around 0.2 g for the 2475-year return period on "rock outcrop" [31]. It is also worth mentioning that the design ground motions are only applicable for a rock level ground. It is expected that the intensity of shaking could be much larger on hill slopes due to topographic amplification and local site response, which could have significant impact on landslide assessment.

Fig. 4(a) presents an elevation map of Hong Kong Island [18]. The study domain is the western part of Hong Kong Island with a dimension of 8 km × 9 km. The area of land is approximately 36 km^2. The highest point is Victoria Peak, which is approximately 552 m above sea level. As shown in Fig. 4(b), rocks in Hong Kong Island primarily consist of volcanic tuff of the Repulse Bay Formation that have been intruded by granite [32]. Due to the subtropical climate, the volcanic and granitic rocks are subjected extensive weathering close to the ground surface. The weathering grade varies from Grade VI (residual soils) on the surface to Grade I (fresh rock) at depth. In the northern sea front close to

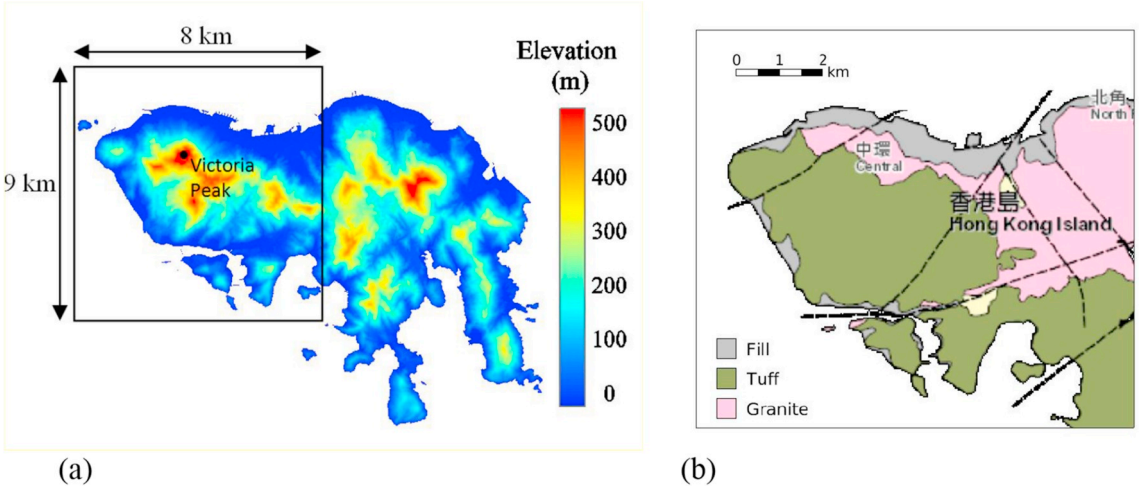

Fig. 4. (a) Hong Kong island and the study region, (b) Bedrock and surficial geology of the study region (adapted from Geological map provided by survey and mapping office, Government of HKSAR).

Victoria Harbour, the land was formed by reclamation (artificial fill).

A digital elevation model at a resolution of 0.5 m×0.5 m is available to extract elevation data in numerical computations, which is fine enough to capture detailed topographic features. The DEM data are provided by the Geotechnical Engineering Office (GEO) of the Civil Engineering and Development Department. Fig. 5(a) illustrates the constructed 3D SEM meshes. The element size is around 20 m × 20 m, which is adjusted to consider the accuracy of high-frequency wave propagation. For the element size of 20 m and shear wave velocity of 200 m/s, the highest frequency that SEM can simulate will be up to 10 Hz because of high-order interpolation scheme used. Fig. 6(b) shows an elevation map with 186 collected boreholes within this area in order to construct subsurface soil strata. Fig. 5(c) illustrates the distribution of slope angles, which generally fall into 30° −45° in the upper part of the hills. Fig. 5(d) shows a map of aspect direction, which is defined as the azimuth direction (0° to 360°) of the steepest downslope, measured clockwise from North. Landslide is assumed to occur along the aspect direction down the slope in computations throughout the study. Accordingly, computed horizontal ground motions need to projected to the aspect direction for Newmark displacement calculation shown in Section 2.2.

To represent realistic soil condition of the study region, 186

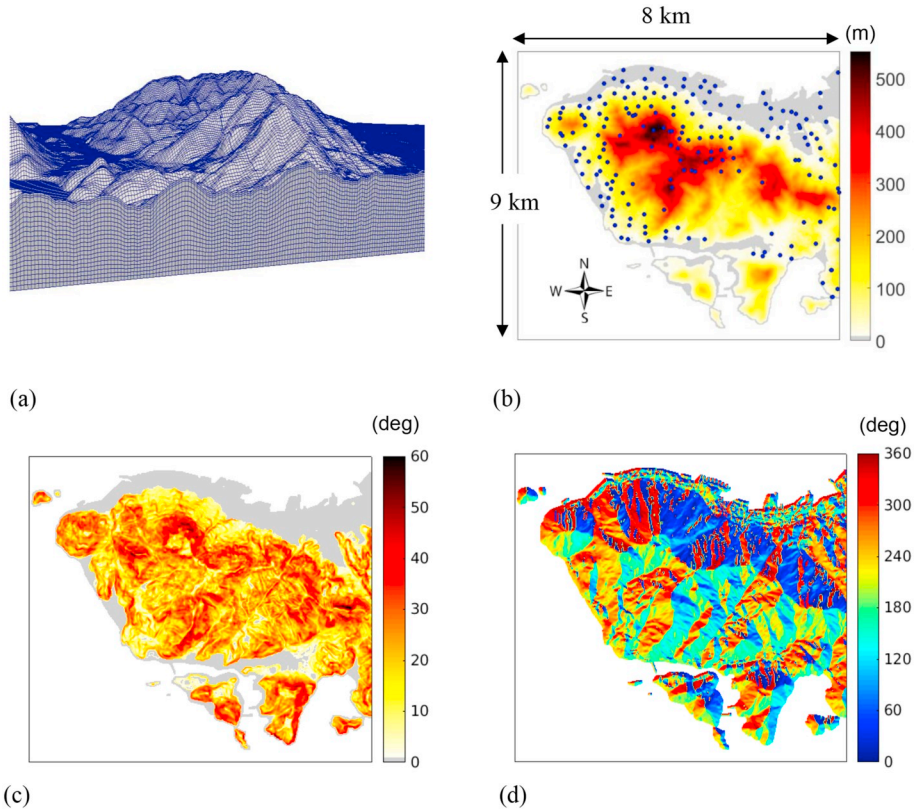

Fig. 5. (a) Illustration of 3D SEM mesh (partial), (b) Distribution of geological boreholes and elevation map, (c) slope angle and (d) aspect direction over the study region.

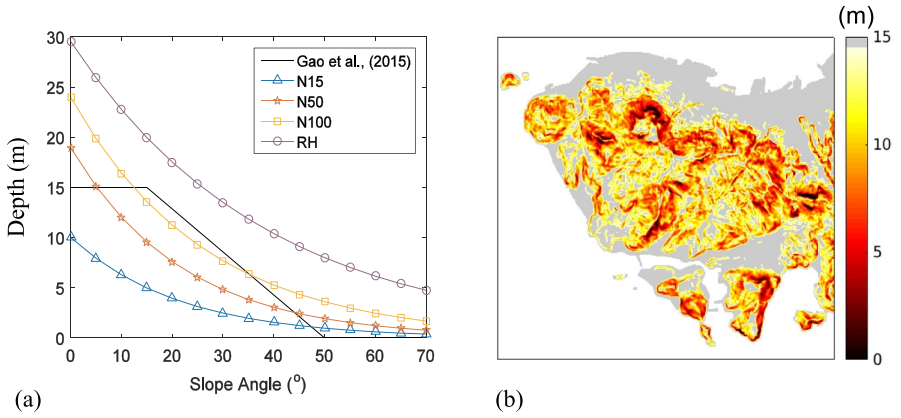

Fig. 6. (a) The relation of soil thickness and slope angle, (b) derived map of soil thickness over the study region.

boreholes shown in Fig. 5(b) are analyzed. Each borehole contains information including ground elevation, geologic units and standard penetration tests (SPT) values at various depths. The abundance of subsurface data makes the study a unique opportunity to construct realistic 3D numerical modelling of regional topography and soil conditions, and to assess region-specific coseismic landslide risks.

Fig. 6(a) summarizes relations derived from borehole data between depths corresponding to a variety of SPT-N values (i.e. N15, N50, N100 and rockhead RH) over the slope angle. These SPT values generally correspond to shear wave velocities of 200, 300, 400 and 1000 m/s, respectively. It can be seen that the soil thickness decreases as slope angle increases. The SPT N100 depth distribution curve is similar to a pervious study of soil thickness model for this area [29], which is therefore used to derive the soil thickness over the study area as shown in Fig. 6(b).

In this study, we assume the soil properties at the sliding surface have an effective frictional angle of 38° and cohesion of 3.5 kPa [29,32]. Hong Kong is featured by its humid sub-tropical climate. During periods of dry weather, soil suction is developed in the soil slope. An average matric suction ψ can be assumed to be −15 kPa based on very limited field monitoring data [28]. Matric suction provides added shear strength to the soil and increases its landslide resistance. On the other hand, water infiltration during heavy rainfall destroys soil suction and increase water table, which significant reduces sliding resistance in the soil. According to study by Geotechnical Engineering Office [28], the likelihood of low, moderate and high degree of saturation in soil slopes is about 95%, 4.5% and 0.5% based on annual rainfall data.

Given these soil parameters and $\psi = -15$ kPa, the static factor of safety (FS) can be calculated for slopes in the study area via Eq. (4), shown in Fig. 7(a). The constant critical acceleration $a_{c,constant}$ can also be derived using Eq. (5), and its distribution is presented in Fig. 7(b). Both of these maps show the safety margin and sliding resistance against earthquake shaking. Ground motions have to exceed the critical acceleration in order to trigger mass movement. In later part of the section, we also evaluate the influence of soil suction and fluctuation of water table on the landside hazard by parametric studies.

3.2. SEM simulation of ground motion amplification

For 3D Spectral Element simulation, the domain is assumed to be bedrock covered by a soil layer. The material is assumed to be viscoelastic with shear wave velocity of 200 m/s for the soil and 1000 m/s for the bedrock respectively. The damping ratios of rock and soil are assigned as 0.5% and 5%, respectively [33]. The soil profile is highly simplified, and more detailed velocity structure can be implemented based on extensive geologic investigation. Yet, significant uncertainty always presents in constructing 3D soil profiles based on limited borehole information, and their effects on ground-motion amplification and landslide should be properly evaluated in future study.

According to a recent PSHA study [31], two dominate scenarios are identified to control the 2457-year return period uniform hazard spectrum (UHS) based on hazard degradation. The first scenario is a near-field earthquake with moment magnitude $M_w = 6$ at a rupture distance R_{rup} of 30 km, which controls the short-period UHS ordinates; the second scenario is a far-field earthquake with $M_w = 8$ at R_{rup} of 300 km that controls the long-period UHS ordinates. The concept of conditional mean spectrum (CMS) [33] is now used to develop target spectra for these two scenarios. Fig. 8(a) shows the resulted CMS of near-field

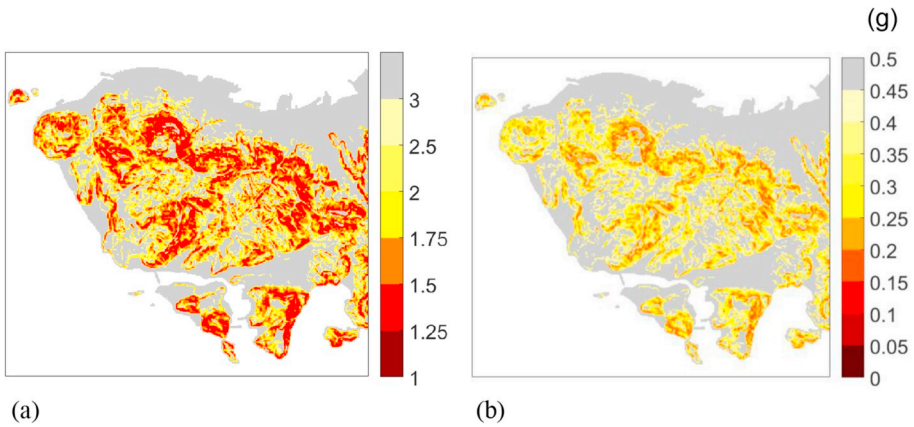

Fig. 7. (a) Static factor-of-safety (FS) map of the studied region; (b) Constant critical acceleration ($a_{c,constant}$) map of the studied region.

scenario (thick dashed line) conditional on 0.1 s, and CMS of far-field scenario (thick dotted line) conditional on 1 s. Ground motions are selected from the Next Generation Attenuation (NGA) database and amplitude scaled to fit these target CMS based on standard procedure [34].

Fig. 8(a) and (b) show the response spectra (PSA) and acceleration time histories of ground motions that fit the near-field CMS with a single scale factor of 1.48 for all three components. Similarly, ground-motion set has been selected for the far-field CMS. Our analysis indicates that the near-field scenario has the dominating effects for landslide hazard analysis. Although the far-field scenario generates long-duration ground motions at the site, the peak ground acceleration is too low (<0.1 g) to trigger landslide. Therefore, only results from near-field ground motions are presented in the following analyses.

Note that the developed ground motions represent the targeted shaking on "rock outcrop". In order to carry out SEM simulation, these outcrop motions are first deconvoluted to the base of the computational domain, then applied as the incidence waves at the base. Lysmer-Kuhlemeyer transmitting boundary is implemented to mimic the infinite rock half space at the bottom of the truncated domain [18], and absorbing boundaries are implemented on the sides to avoid artificial wave reflection [35]. Finally, three-component ground motion computed within the sliding mass are recorded in order to compute "equivalent acceleration" for the Newmark sliding displacement analysis.

Fig. 9 shows the peak ground acceleration (PGA) map resulted from the 3D SEM simulation. Note that the reference PGA on rock outcrop is around 0.2 g in the W-E direction and 0.1 g in the vertical direction, respectively, as specified in Fig. 8. As shown in Figs. 9 and 11(a), significant PGA amplification can be observed in the horizontal and vertical directions due to combined effects of topographic amplification and local site response, which will be discussed in detail below. The maximum horizontal PGA reaches up to 1.2 g at protruded local areas and top of ridges with a total amplification factor of 4–6.

For comparison, 3D SEM simulation is also performed on a hypothetical homogenous rock model (Vs = 1000 m/s) without the soil layer. For this case, the PGA distribution is shown in Fig. 10 and Fig. 11(b), which is solely due to topographic amplification. It can be observed that the spatial distribution pattern of PGA on the homogenous rock site is closely related to smoothed curvature of the topography [18]. Due to focusing and defocusing effect, PGA is amplified or deamplified at locally protruded or concaved areas, yet, the maximum topographic amplification factor is less than 2. The comparison concludes that strong amplification in Fig. 9 is controlled in the first place by velocity structure of the soils, and it cannot be explained only by topography.

On the other hand, 1D site response analyses are performed to assess the 1D soil amplification effect. When thickness of the soil layer increases from 0 to 20 m, 1D amplification factor of PGA on the soil increases from 1.0–1.5 against the reference PGA on rock outcrop. By contrast, based on 3D DEM simulations, the ratios of PGAs on the layered soil v.s. on the uniform rock are notably much larger (up to 6) than the 1D soil amplification factor, as shown in Fig. 11(c). It clearly demonstrates that the total amplification on the layered soil (Fig. 9) is much more pronounced than direct superposition of topographic effects and 1D soil amplification. It is worth pointing out that, although numerical simulations have been extensively conducted in the past, most of these analyses are performed by assuming simple topography and uniformly distributed materials, which tend to greatly underestimates some of the observed field data [36,37]. This study demonstrates the importance of modeling heterogeneous soil distribution realistically based on detailed geological investigation in order to capture the combined effects of topography and soil response. Accurate prediction of ground motions is obviously most important for ensuing coseismic landslide calculation.

3.3. Coseismic landslide analyses

Fig. 12 summarizes the potential sliding area under the four computational cases: (*i*) the input motion is 2D in horizontal directions using $a_{c,constant,}$ (*ii*) the input motion is 3D shaking (including vertical motion) using $a_{c,constant,}$ (*iii*) 2D horizontal shaking using $a_{c,transient,}$ (*iv*) 3D shaking using $a_{c,transient}$. For 2D shaking input, two horizontal accelerations are used in Newmark calculation, while for 3D shaking input, three component accelerations are used in Newmark analyses. It is seen that by using transient critical acceleration $a_{c,transient}$ and 3D shaking, it yields largest sliding displacement. The area of exceedance of different Newmark displacement values for different cases is shown in Fig. 12(b). For example, the area with Newmark displacement larger than 1 cm is around 0.72 km^2 for case (*ii*). If 5 cm is adopted as the critical value for regional earthquake-induced landslide assessment, the total sliding area for case (*iv*) using $a_{c,transient}$ and 3D shaking is 0.19 km^2, which is larger than sliding area of 0.06 km^2 for case (*i*) using $a_{c,constant,}$ under horizontal shaking. Note that if the vertical motion is accounted for in computation, the sliding area increases approximately 15%.

As discussed before, degree of soil saturation changes significantly during dry and rainfall seasons. Water table fluctuates over the seasons under different rainfall infiltration and drainage. Therefore, the hydrogeological condition becomes one of the most significant factors in assessing coseismic landslide hazards in Hong Kong. As shown in Fig. 13, Newmark displacement significantly increase across the terrain when the soil is submerged as compared with the unsaturated case. Fig. 14 summarizes the influence of matric suction and water table location on the area of sliding. Note that parameter *m* is used to indicate the proportion of sliding mass that is submerged under water table. It is evident that *m* affects the landslide hazard significantly. As shown in Fig. 14(b), if 5 cm of Newmark displacement is adopted as a threshold value for

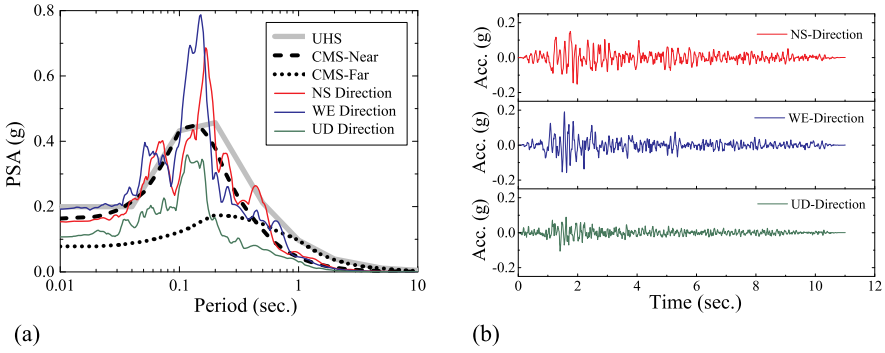

Fig. 8. (a) Target conditional mean spectrum (CMS) and uniform hazard spectrum (UHS) for rock outcrop in Hong Kong, showing response spectra of scaled motions in three directions; (b) three-component motions scaled by 1.48, recorded at Anza-Red Mountain station during the 1986 North Palm Springs earthquake. (For interpretation of the references to colour in this figure legend, the reader is referred to the Web version of this article.)

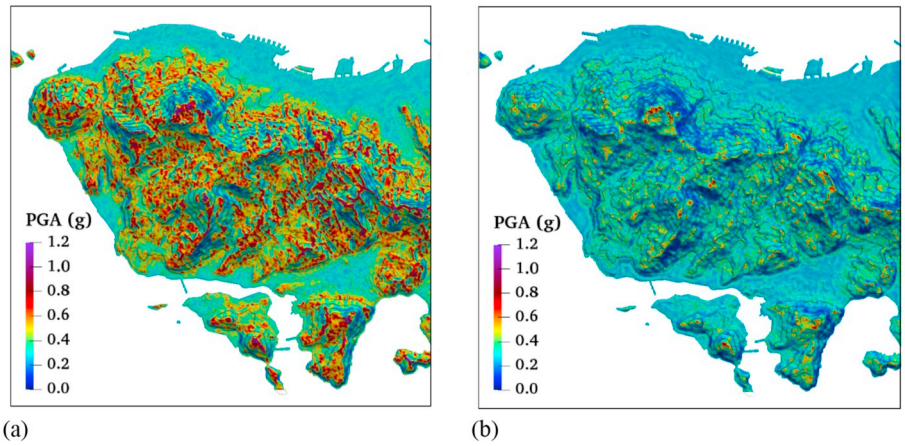

Fig. 9. Amplification of peak ground accelerations due to topography and site response. (a) Horizontal (W–E) direction, (b) Vertical direction. Elevation contour lines starts from sea level (0 m) with a 50 m interval.

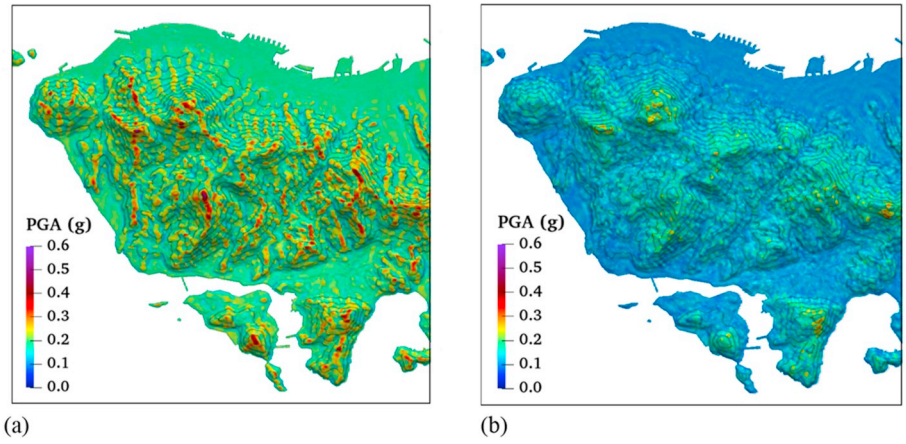

Fig. 10. Amplification of peak ground accelerations on a hypothetical uniform rock site. (a) Horizontal (W–E) direction, (b) Vertical direction. Elevation contour lines starts from sea level (0 m) with a 50 m interval.

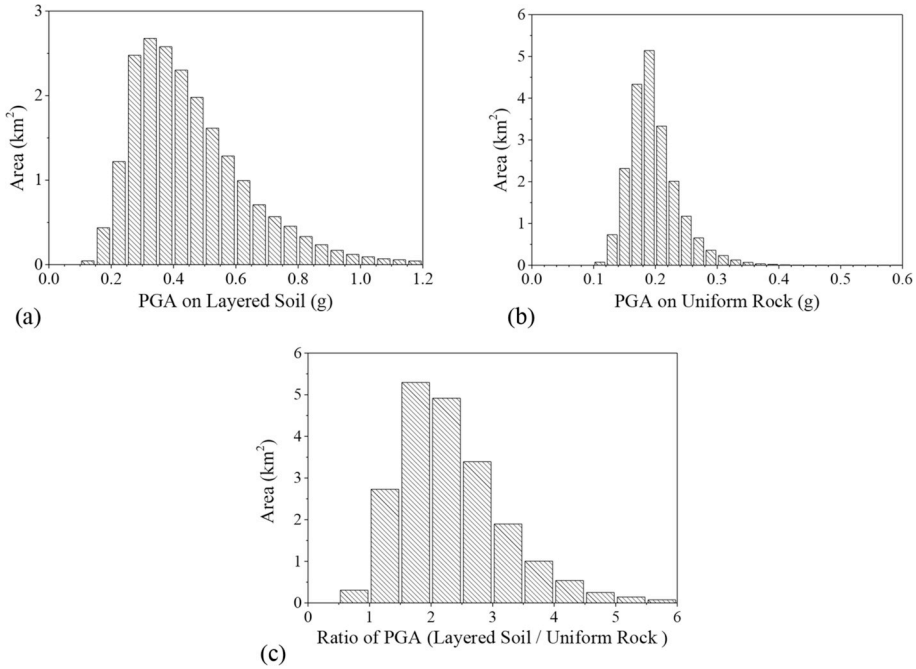

Fig. 11. Horizontal PGA (W-E component) distribution on (a) the layered soil v.s. (b) The uniform rock, and (c) their ratios.

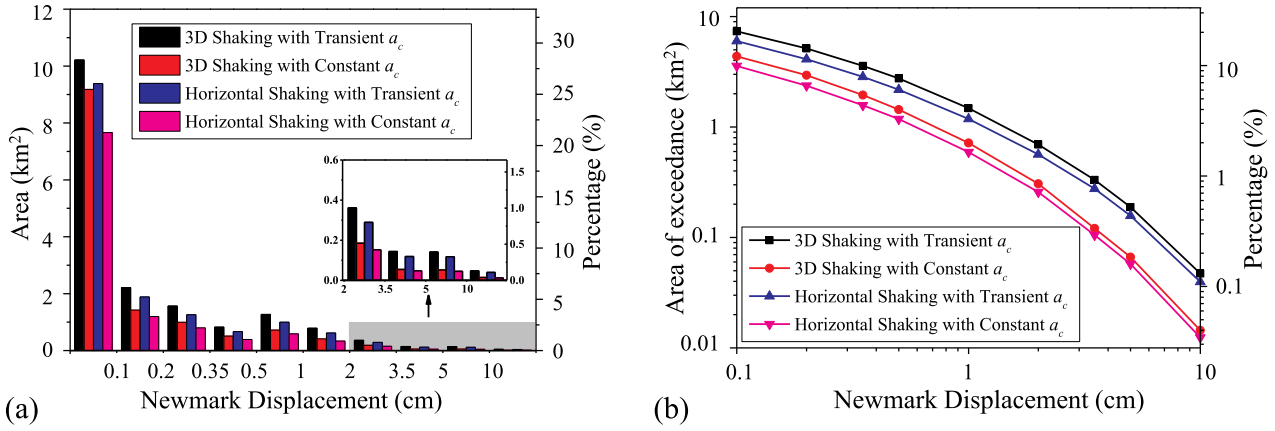

Fig. 12. (a) Potential sliding area and percentage of Newmark displacement, (b) area of exceedance and percentage of different Newmark displacement using different computational cases.

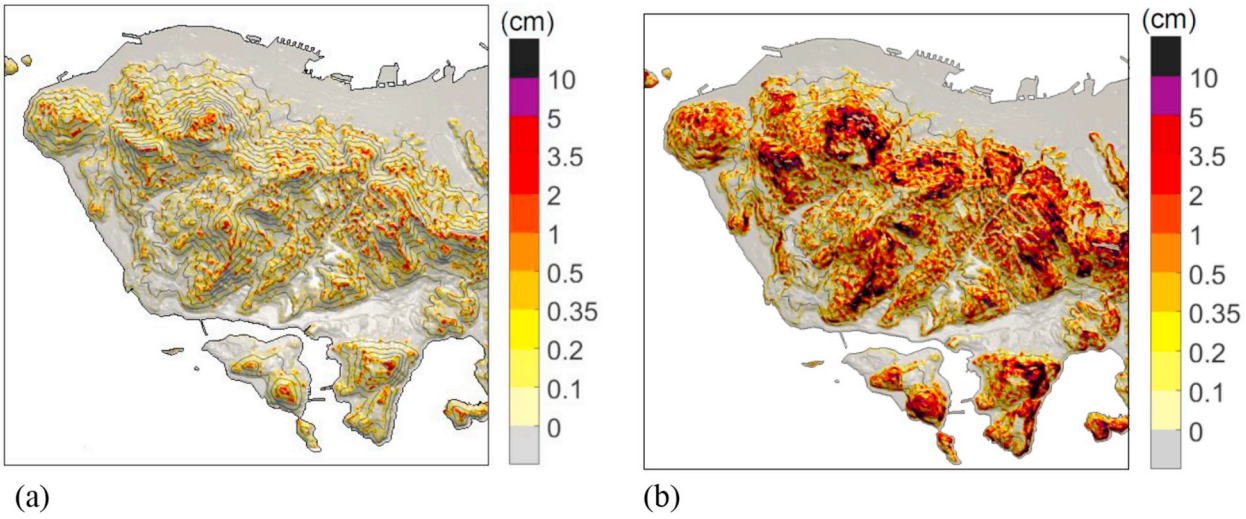

Fig. 13. Newmark displacement maps computed using 3D $a_{c,transient}$ under three-component input motions for (a) unsaturated case, suction $\psi = -15$ kPa, and (b) submerged case, $m = 0.1$.

triggering of landslide, the total sliding area for the unsaturated case (suction −15 kPa) is 0.19 km^2. Yet, the sliding area notably increases to 1.4 km^2, 2.5 km^2, 6.3 km^2 and 12.3 km^2 when the water table rises (m = 0, 0.1, 0.3, 0.5).

In the following part, the slope failure probability map over the study region is derived. Given that case histories of the seismically induced slope failure in Hong Kong is lacking, an empirical relation based on California slope failure data [26] is adopted in the current study, as shown in Eq. (7):

$$P(f) = 0.335\left[1 - \exp\left(-0.048 D_n^{1.565}\right)\right] \quad (7)$$

where $P(f)$ denotes the probability of slope failure, and D_n is the Newmark displacement in centimeters. By using this equation, the slope failure probability can be generated using the Newmark displacement map. It can be seen from Fig. 14(c) that there is about 1% of the total area with probability of failure greater than 10% if the sliding surface is unsaturated (suction 15 kPa). The 10% sliding probability area quickly increases to 5%, 9%, 20% and 40% when the water table rises (m = 0, 0.1, 0.3, 0.5), showing the hydrological condition is one of the most important factors in assessing sliding hazard. The results emphasize the importance of incorporating three-dimensional topographic features and ground shaking in coseismic landslide assessments.

4. Hongshiyan landslide during the 2014 Ludian earthquake

4.1. Regional-scale SEM model

The second case study in this paper assesses the regional-scale Hongshiyan landslide during the 2014 M6.5 Ludian earthquake in China using the SEM-Newmark method. Among numerous landslides triggered during the earthquake, the Hongshiyan landslide located along the Niulan River, 10 km away from the earthquake epicenter, is the largest [38]. A sliding mass of approximately 12 million m^3 avalanched into the V-shaped canyon and blocked the river flow. Fig. 15(a) and (b) show the regional topography and the Hongshiyan landslide site. Slope height close to the river channel is around 600 m, with a slope angle of 50–60° along the right bank and 35–50° along the left bank. The lithology of the landslide is featured by Devonian limestone and dolomite overlying Ordovician mudstone and shale. Rocks on the slope surface are heavily fractured, and a strong weathered profile reaches 20–30 m in depth. Under the earthquake loading, extensive fractures were developed in the rock masses. The loosened materials slided down along the steep terrain into the river and formed a 116 m high barrier dam [39].

Seismology investigation reveals that the fault mechanism is left-lateral strike-slip faulting. In the SEM simulation, we adopted the fault

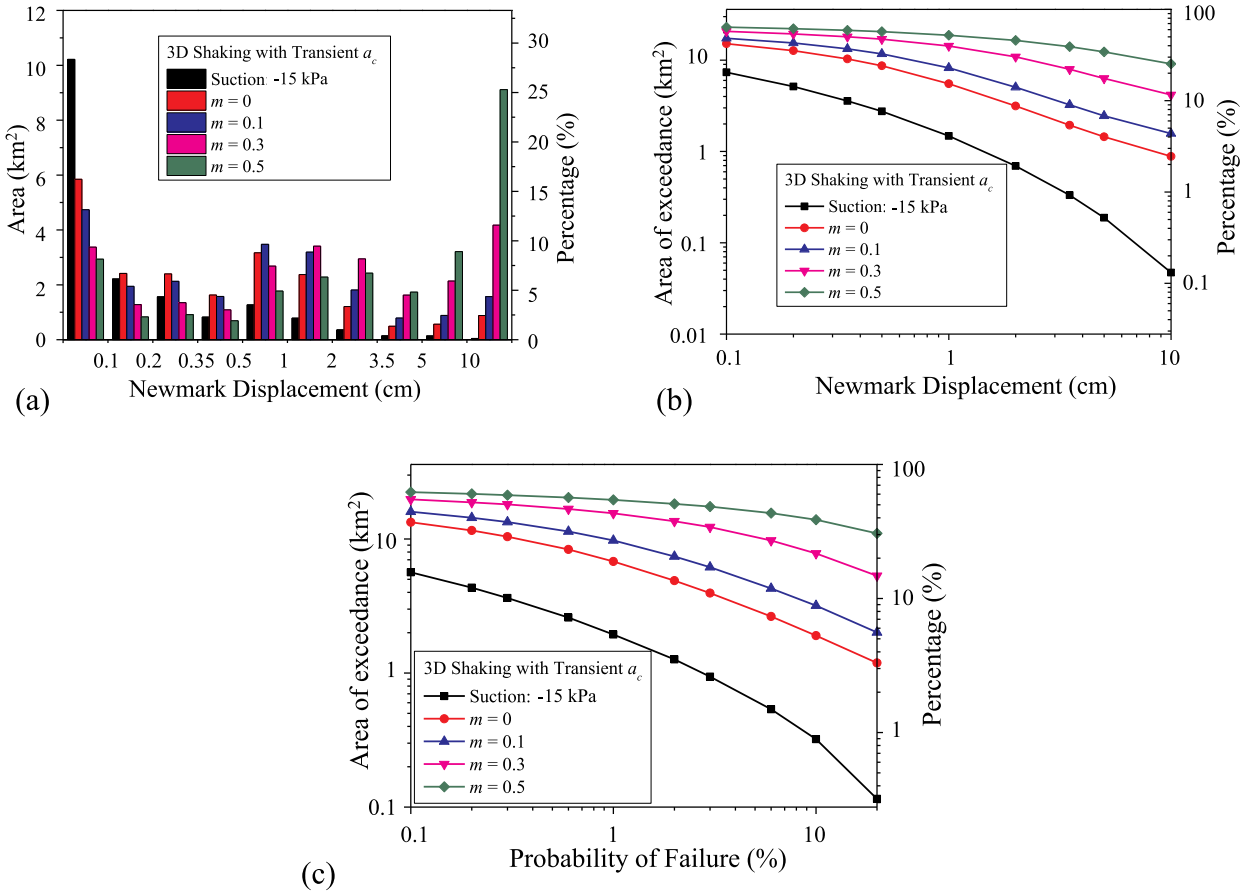

Fig. 14. Influence of water table on (a) sliding area and percentage of Newmark displacement, (b) area of exceedance and area percentage of different Newmark displacement using different computational cases, (c) probability of failure.

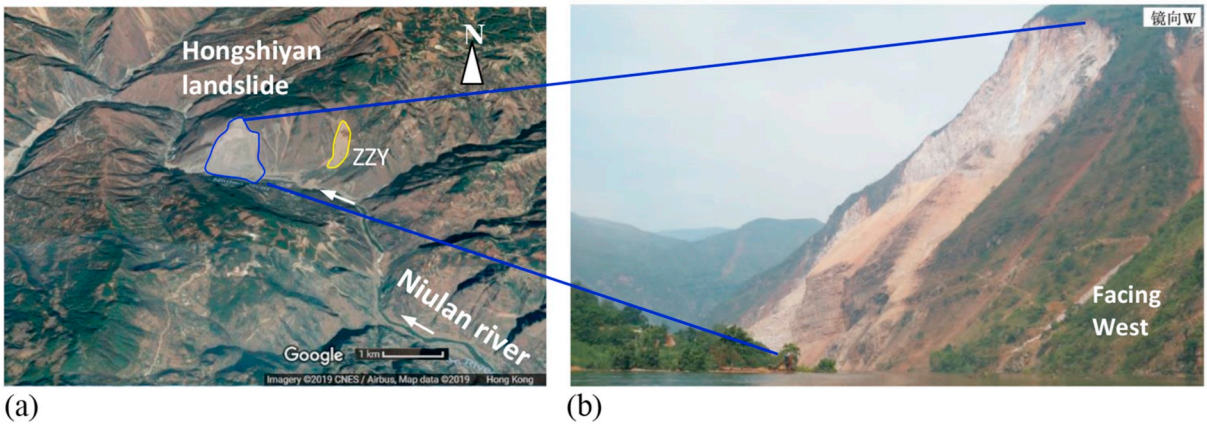

Fig. 15. The Hongshiyan (HSY) landslide triggered in the 2014 M6.5 Ludian earthquake in China: (a) Topography of the Hongshiyan region, from Google Earth; (b) Hongshiyan (HSY) landslide site facing towards west, from Ref. [37].

rupture model derived from finite fault inversion using regional broadband data [40]. As can be seen from Fig. 16 (a), the majority of the rupture slip was concentrated within a shallow depth of less than 10 km, while the maximum rupture slip was at a depth of 3 km, thus it generated very strong ground shaking over the region. Fig. 16 (b) shows the energy release rate of the fault rupture, where most of energy release is within the first 10 s. Fig. 16 (c) is an elevation map of the Ludian county, also showing the horizontal projection of the fault plane (red line) of the **M**6.5 Ludian earthquake. Three locations are highlighted with solid triangles for our future study. The HSY is the Hongshiyan landslide site, ZZY is another smaller scale landslide nearby (also see Fig. 15(a)). Fortunately, a seismograph station is located at LLT within this region. The recorded motions at the station will be used to validate the numerical simulation. Distribution of the slope angle is illustrated in Fig. 16(d).

A region-scale SEM simulation is carried out to quantify the Newmark sliding displacement in the region in response to the Ludian earthquake. As shown in Fig. 17(a), the dimension of the SEM computational domain was 17.8 km × 26.6 km × 18 km. A high-resolution digital elevation model was utilized to construct detailed topographic

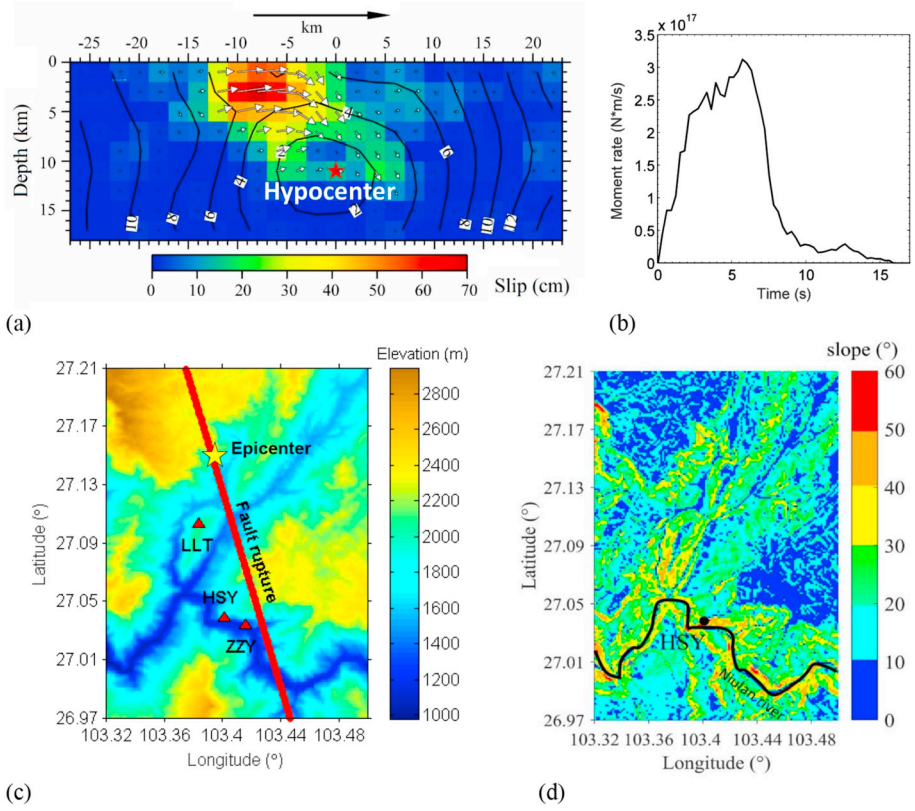

Fig. 16. (a) Fault rupture model, showing the slip amount (in cm) and rupture propagation contours (in s) (after [40]), (b) energy release rate of the fault rupture, (c) Elevation of the study region, showing the horizontal projection of the fault line (red line) and epicenter of the 2014 **M**6.5 Ludian earthquake, and (d) slope angle distribution of the terrain. (For interpretation of the references to colour in this figure legend, the reader is referred to the Web version of this article.)

feature. Variation of shear wave velocity along the depth is illustrated in Fig. 17(b). Near surface material properties are estimated from a geological survey, with a friction angle of 35°∼45° and cohesion of 1–2 MPa [39]. Since post-earthquake reconnaissance demonstrates that ground water table in Hongshiyan landslide area is considerably lower than the sliding surface, so the sliding material is assumed to be dry in Newmark analysis. Transmitting boundary is implemented at the bottom and the sides of the domain to avoid wave reflection into the domain [41].

4.2. *Wave propagation and coseismic landslide analyses*

Fig. 18 illustrates the distribution of simulated wave propagation pattern on the ground surface. During the event, the seismic waves propagates from the rupture towards the HSY site, which falls within the forward directivity region. Fault rupture propagation and earthquake source radiation cause spatial variation of ground motion in amplitude and duration around the fault plane. In addition, large-amplitude velocities are concentrated at the HSY site at around 7.5 s, due to topographic amplification of the ground motion by the steep terrain along the right bank of the river. Note that large velocity is absent just across

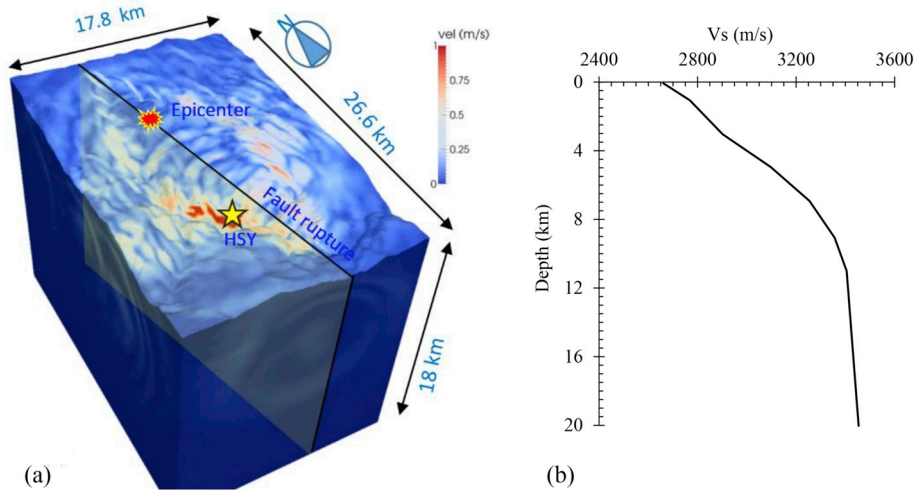

Fig. 17. SEM simulated wave field during the 2014 Ludian earthquake (a) computational domain (b) shear wave velocity profile.

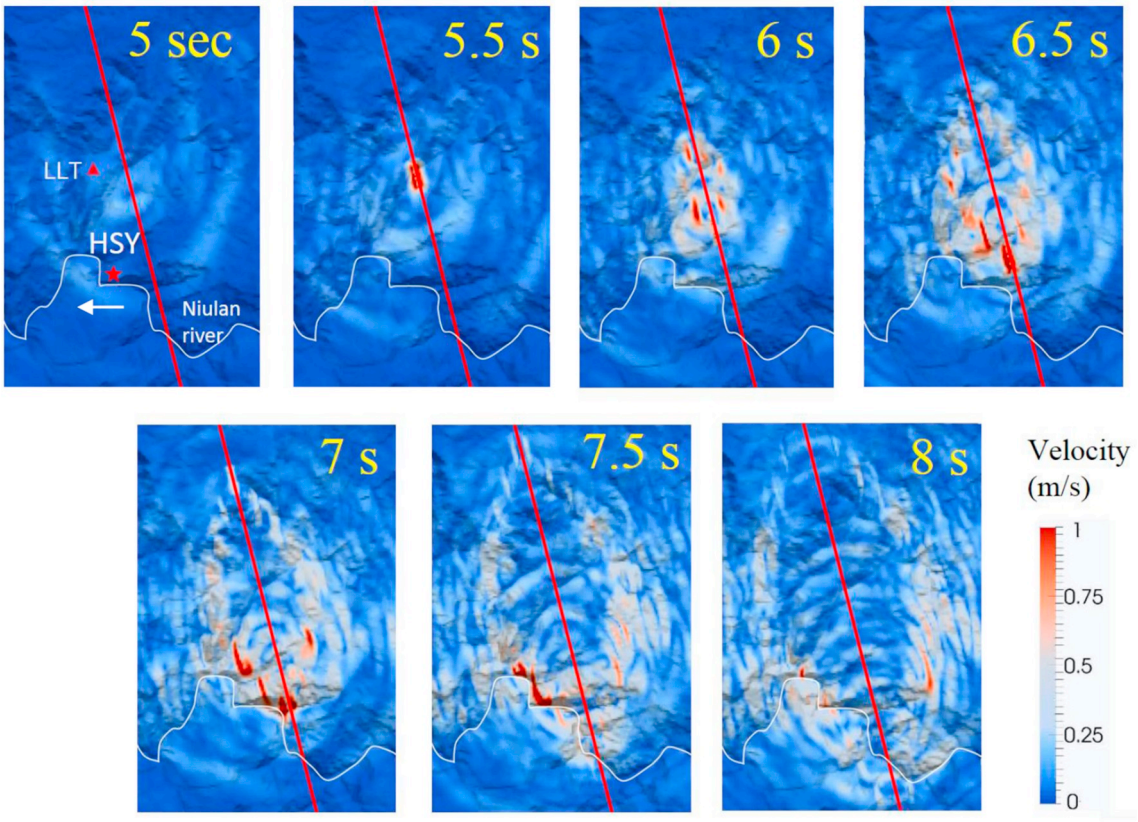

Fig. 18. Simulated wave propagation pattern and ground velocity over the study region from 5 s to 8 s.

the river at the left bank because the slope angle is much flatter.

To validate the SEM model, thorough comparison between simulated and recorded ground motions at a near source site, the LLT station is provided. Note that epicenter distance of the LLT station is approximately 5 km, where a large peak ground velocity of approximately 0.7 m/s was recorded during the 2014 Ludian event. Fig. 19 presents acceleration and velocity time histories in E-W, N–S, and vertical directions, as well as Fourier and response spectra for simulated and recorded motions at the LLT station (Fig. 20). By visual inspection, the simulated and recorded velocity time histories are very similar in terms of both time and frequency characteristics, peak amplitude and duration. In general, the simulation captured the overall feature of a near-source motion reasonably well.

Fig. 21 presents simulated acceleration, velocity and displacement

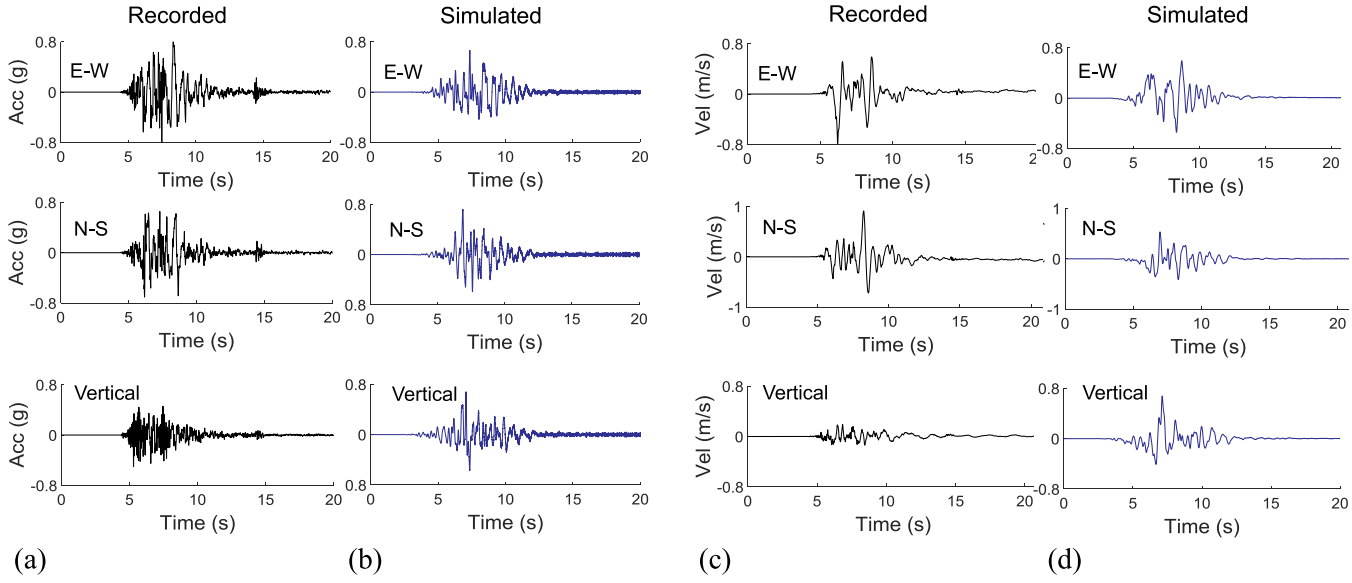

Fig. 19. Recorded and simulated (a) (b) acceleration and (c) (d) velocity time histories in E-W, N–S, and vertical directions at the LLT station during the Ludian earthquake.

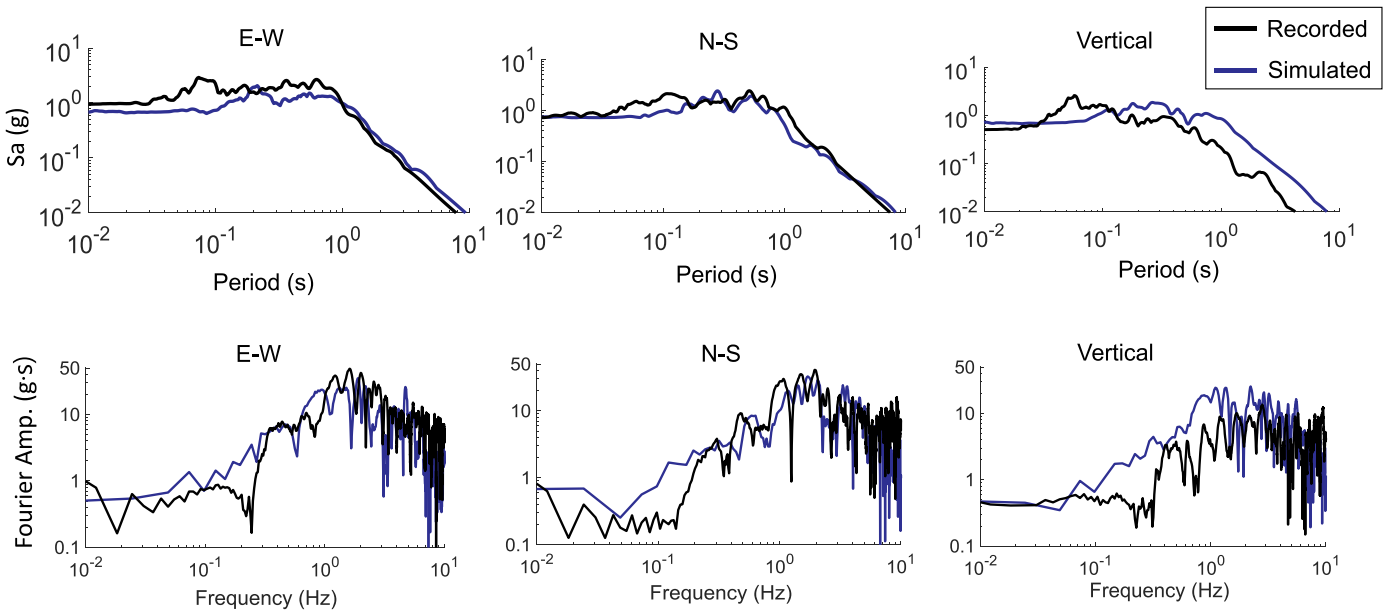

Fig. 20. Comparison of response spectra and Fourier spectra of simulated and recorded motions at LLT station during Ludian earthquake.

time histories in the E-W, N–S and vertical directions at the HSY site. As suggested by Somerville et al. [42], near-fault motions usually contain strong velocity pulses that may be associated with rupture directivity effects. Such velocity pulses would impose severe demand on structures and geotechnical systems. It was identified by previous researchers that earthquake motions with fling effects would excite structural systems essentially in their fundamental mode while recordings with forward directivity in the absence of fling activate higher modes of vibration. In this study, the simulated motion at the Hongshiyan landslide site does contain a large velocity pulse with a peak value greater than 100 cm/s, indicating that the spectral element simulation captures the near-fault and forward-directivity ground-motion features reasonably well. In the meantime, the fling effect, being a result of the evolution of residual ground displacement due to tectonic deformation associated with rupture mechanism [43], is observed in the simulated displacement time histories. A fling step as much as 0.3 m is accumulated in the N–S direction at the end of ground shaking.

Following the integrated SEM-Newmark scheme proposed in this study, peak velocity distribution and major landslides in the study region triggered by the 2014 Ludian earthquake are simulated and identified in Fig. 22. Fig. 22(b)(c) show the distribution of Newmark sliding displacement when peak-strength and residual-strength parameters are used for the subsurface materials in estimation. It can be observed that the predicted displacement at the HSY site is 40 cm. Note that 40 cm is the predicted Newmark displacement using the peak strength of the sliding material (a friction angle of 38° and cohesion of 1 MPa), which can only be used as an index to determine the triggering of a landslide. Based on widely accepted criterion [26], a Newmark displacement of 40 cm well indicates triggering of a major landslide. To estimate the sliding distance kinematically, the residual rock strength (friction angle 30°, cohesion of 20 kPa) is used in Newmark analysis (Fig. 22(c)), and the resulted sliding displacement at Hongshiyan site is approximately 800 m, indicating a long-distance sliding would occur once the landslide is triggered and the material strength is degradated in large deformation.

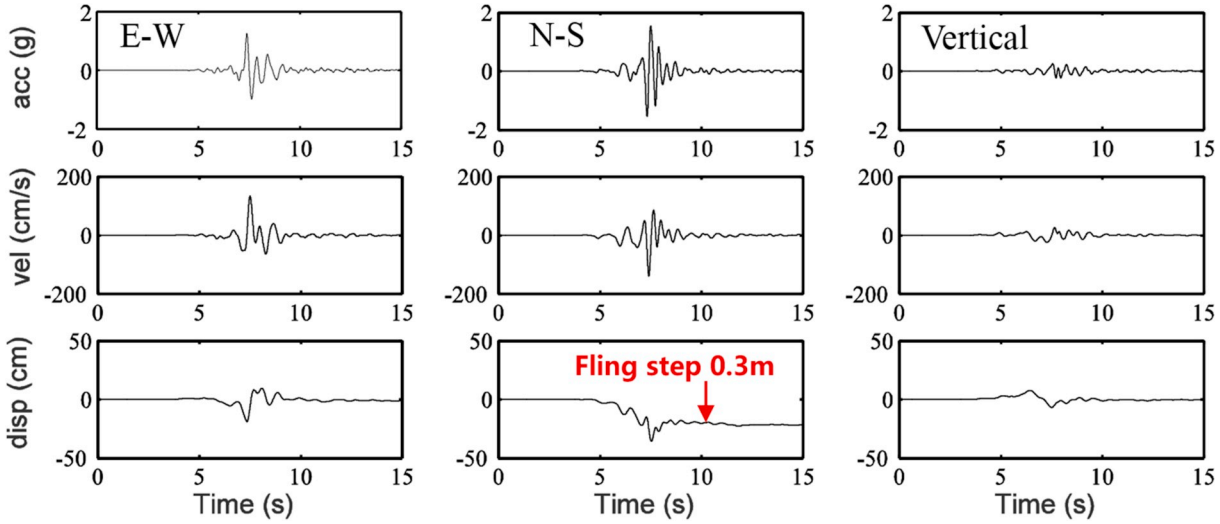

Fig. 21. Simulated acceleration, velocity and displacement time histories in the E-W, N-Sand vertical directions at the Hongshiyan (HSY) landslide site.

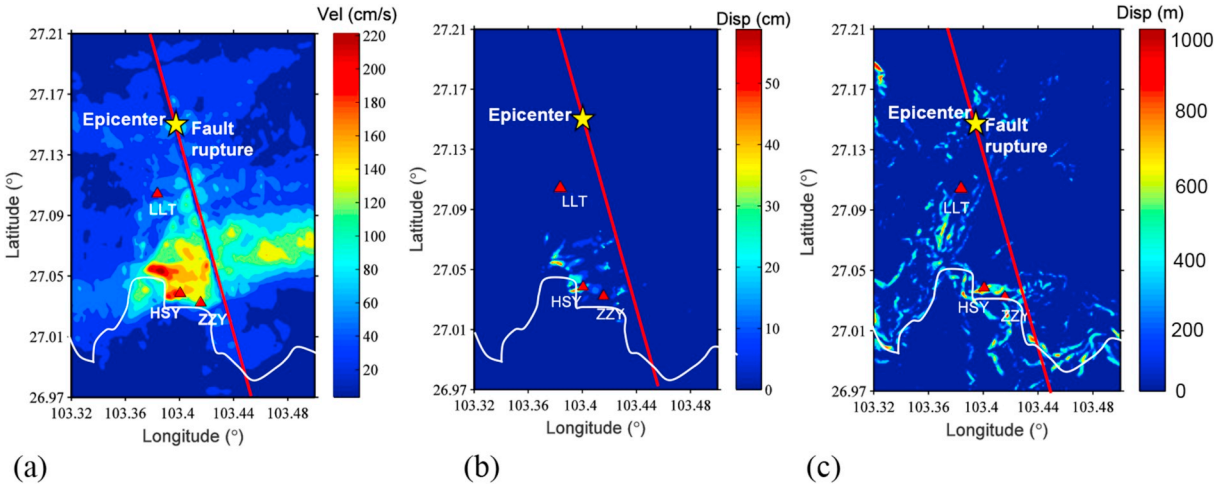

Fig. 22. (a) Peak velocity distribution, and estimated Newmark sliding displacement during the 2014 Ludian earthquake at the Hongshiyan landslide site in a regional scale using (b) peak strength and (c) residual strength parameters.

5. Discussions and conclusions

In this study, a new integrated model is presented that allows for direct simulation of the coseismic landslide process using the Spectral Element Method (SEM) and Newmark sliding displacement analyses. On the regional scale, the SEM is capable of modeling 3D seismic wave fields in complex topography at a scale of hundreds of kilometers, and thus capture a big picture of earthquake strikes and associated landslide hazards. Distinctive features of near-fault ground motions, such as large velocity pulses and directivity effects can be faithfully simulated. On the local scale, Newmark displacement model considers key factors such as material strength, geometry, and degree of soil saturation. These effects are usually difficult to quantify using empirically-based methods, but it is well noted that the characteristics of spatially distributed ground motions as well as regional site conditions would significantly affect triggering of landslides [13,14]. The integrated SEM-Newmark method provides the first-of-its-kind numerical tool for integrated study of regional-scale landslides under earthquake shaking.

Case studies are conducted to assess regional-scale landslide risks in the western part of Hong Kong island and the massive landslide occurred during the 2014 M6.5 Ludian earthquake in Yunnan province, China. The Hong Kong study emphases on the influence of topographic amplification, soil response and varying hydrogeological conditions in dry and rainfall seasons. The sliding mass is relatively shallow. Emphasis has been placed on modeling heterogenous subsurface soil in order to capture complicated ground-motion amplification due to combined effects of topography and soil amplification. On the other hand, the Hongshiyan landslide case is featured by deep-seated sliding that was triggered by strong near-source motions and topographic effects. By using“equivalent accelerations” in Newmark calculation, both shallow and deep sliding can be simulated. These case studies confirm the effectiveness of the proposed method for a regional scale analysis.

In summary, the paper demonstrates great promise of using the physics-based broadband earthquake simulation integrated with the Newmark method in modeling the regional scale seismic landslide process. The integrated numerical model can find important applications in systematically studying coseismic landside processes using a large amount of earthquake scenarios and hydrogeologic conditions. Following this line, empirical seismic landslide prediction models could be developed based on direct simulation, which would refine and improve current empirical prediction models. Machine learning and big-data analytics could also be used for investigating these data [44]. On the other hand, it should be emphasized that landslide triggering mechanism and flow dynamics are very complicated phenomena. The present integrated method is limited to the case of mass sliding with a pre-defined sliding surface. Many other features such as strong nonlinearity and internal structure of subsurface materials, groundwater fluctuation and seepage, may also be crucial to coseismic landslides, but they have not yet been considered. With the advancement of computational technology, there is an opportunity to develop advanced numerical model, such as the Material Point Method [45], to study the progressive slope failure process and post-failure large deformation behavior, including triggering, runoff and deposition of landslide masses. These possibilities illustrate that there will be sufficient potential for future research. More importantly, more case history studies need to be conducted to calibrate and validate these numerical models [46], and provide more insights into this topic.

Declaration of competing interest

All authors state that there are no interests to declare.

CRediT authorship contribution statement

Duruo Huang: Conceptualization, Methodology, Project administration, Writing - original draft, Writing - review & editing. **Gang Wang:** Methodology, Supervision, Funding acquisition, Writing - review & editing. **Chunyang Du:** Software, Formal analysis, Writing - original draft. **Feng Jin:** Methodology, Data curation. **Kewei Feng:** Software, Formal analysis. **Zhengwei Chen:** Formal analysis.

Acknowledgements

The authors acknowledge support from Joint Research Fund for Overseas Chinese Scholars and Scholars in Hong Kong and Macau Grant No. 51828902 and project Grant No. 51639006 from the National Natural Science Foundation of China (NSFC), and General Research Fund Grant No. 16214118 from the Hong Kong Research Grants Council.

References

[1] Harp EL, Jibson RW. Landslides triggered by the 1994 Northridge, California, earthquake. Bull Seismol Soc Am 1996;86(1B):S319–32.
[2] Yin YP, Wang FW, Sun P. Landslide hazards triggered by the 2008 Wenchuan earthquake, Sichuan, China. Landslides 2009;6:139–52.
[3] Jibson RW. Regression models for estimating coseismic landslide displacement. Eng Geol 2007;91:209–18.
[4] Rathje EM, Saygili G. Probabilistic seismic hazard analysis for the sliding displacement of slopes: scalar and vector approaches. J Geotech Geoenviron Eng 2008;134(6):804–14.

[5] Du W, Wang G. Fully probabilistic seismic displacement analysis of spatially distributed slopes using spatially correlated vector intensity measures. Earthq Eng Struct Dynam 2014;43(5):661–79.
[6] Du W, Wang G, Huang D. Influence of slope property variabilities on seismic sliding displacement analysis. Eng Geol 2018;242:121–9.
[7] Du W, Wang G, Huang D. Evaluation of seismic slope displacement based on fully coupled sliding mass analysis and NGA-West2 database. ASCE J Geotech Geoenviron Eng 2018;144(8):06018006.
[8] Du W, Huang D, Wang G. Quantification of model uncertainty and variability in Newmark displacement analysis. Soil Dynam Earthq Eng 2018;109:286–98.
[9] Kokusho T. Energy-based Newmark method for earthquake-induced slope displacement. Soil Dynam Earthq Eng 2019;121:121–34.
[10] Jibson RW. Methods for assessing the stability of slopes during earthquakes—a retrospective. Eng Geol 2011;122:43–50.
[11] Rathje Ellen M, George Antonakos. A unified model for predicting earthquake-induced sliding displacements of rigid and flexible slopes. Eng Geol 2011;122:51–60.
[12] Baker JW. Quantitative classification of near-fault ground motions using wavelet analysis. Bull Seismol Soc Am 2007;97:1486–501.
[13] Huang D, Wang G. Stochastic simulation of regionalized ground motions using wavelet packets and cokriging analysis. Earthq Eng Struct Dynam 2015;44(5):775–94.
[14] Huang D, Wang G. Region-specific spatial cross-correlation model for stochastic simulation of regionalized ground-motion time histories. Bull Seismol Soc Am 2015;105(1):272–84.
[15] Huang D, Wang G. Energy-compatible and spectrum-compatible (ECSC) ground motion simulation using wavelet packets. Earthq Eng Struct Dynam 2017;46:1855–73.
[16] Assimaki D, Jeong S. Ground-motion observations at Hotel Montana during the M7.0 2010 Haiti earthquake: topography or soil amplification? Bull Seismol Soc Am 2013;103(5):2577–90.
[17] Asimaki D, Mohammadi K. On the complexity of seismic waves trapped in irregular topographies. Soil Dynam Earthq Eng 2018;114:424–37.
[18] Wang G, Du C, Huang D, Jin F, Koo RCH, Kwan JSH. Parametric models for 3D topographic amplification of ground motions considering subsurface soils. Soil Dynam Earthq Eng 2018;115:41–54.
[19] Song J, Rodriguez-Marek A. Sliding displacement of flexible earth slopes subject to near-fault ground motions. J Geotech Geoenviron Eng 2015;141(3):04014110.
[20] Tsai CC, Lin CH. Prediction of earthquake-induced slope displacements considering 2D topographic amplification and flexible sliding mass. Soil Dynam Earthq Eng 2018;118:25–34.
[21] Komatitsch D, Vilotte JP. The spectral element method: an efficient tool to simulate the seismic response of 2D and 3D geological structures. Bull Seismol Soc Am 1998;88(2):368–92.
[22] Komatitsch D, Tromp J. Introduction to the spectral element method for three-dimensional seismic wave propagation. Geophys J Int 1999;139(3):806–22.
[23] Savage B, Komatitsch D, Tromp J. Effects of 3D attenuation on seismic wave amplitude and phase measurements. Bull Seismol Soc Am 2010;100(3):1241–51.
[24] Tsai CC, Lin CH. Prediction of earthquake-induced slope displacements considering 2D topographic amplification and flexible sliding mass. Soil Dynam Earthq Eng 2018;113:25–34.
[25] Rathje EM, Antonakos G. A unified model for predicting earthquake-induced sliding displacements of rigid and flexible slopes. Eng Geol 2011;122:51–60.
[26] Jibson RW, Harp EL, Michael JA. A method for producing digital probabilistic seismic landslide hazard maps. Eng Geol 2000;58:271–89.
[27] Cho SE, Lee SR. Evaluation of surficial stability for homogeneous slopes considering rainfall characteristics. J Geotech Geoenviron Eng 2002;128(9):756–63.
[28] GEO. Preliminary quantitative risk assessment of earthquake-induced landslides at man-made slopes in Hong Kong. GEO Report No. 98, Geotechnical Engineering Office. Hong Kong SAR: Civil Engineering Department; 1998.
[29] Gao L, Zhang LM, Chen HX. Likely scenarios of natural terrain shallow slope failures on Hong Kong Island under extreme storms. Nat Hazards Rev 2015;18:B4015001.
[30] Mok HY, Koo RCH, Kwan JSH, Lau DS. Earthquake monitoring and probabilistic seismic hazard assessment of Hong Kong. Hong Kong: Geotechnical Engineering Office, Civil Engineering and Development Department; 2012. Reprint 1175.
[31] GEO. Seismic hazard analysis of the Hong Kong region. GEO report No. 311, geotechnical engineering office. Hong Kong SAR: Civil Engineering Department; 2015.
[32] GCO. Mid-levels study: report on geology, hydrology and soil properties. Hong Kong: Geotechnical Control Office, Government of Hong Kong SAR; 1982.
[33] Baker JW. Conditional mean spectrum: tool for ground-motion selection. J Struct Eng 2011;137(3):322–31.
[34] Wang G, Youngs R, Power M, Li Z. Design ground motion library: an interactive tool for selecting earthquake ground motions. Earthq Spectra 2015;31:617–35.
[35] Wang G, Sitar N. Static and dynamic axial response of drilled piers. II: numerical simulation. J Geotech Geoenviron Eng 2011;137(12):1143–53.
[36] Massa M, Barani S, Lovati S. Overview of topographic effects based on experimental observations: meaning, causes and possible interpretations. Geophys J Int 2014;197:1537–50.
[37] Jeong S, Asimaki D, Dafni J, Wartman J. How topography-dependent are topographic effects? Complementary numerical modeling of centrifuge experiments. Soil Dynam Earthq Eng 2019:654–67.
[38] Li X, Xu X, Ran Y, Cui J, Xie Y, Xu F. Compound fault rupture in the 2014 Ms 6.5 Ludian, China, earthquake and significance to disaster mitigation. Seismol Res Lett 2015;86(3):764–74.
[39] Chen XL, Chang ZF, Wang K. Numerical simulation of Hongshiyan landslide triggered by the Ms 6.5 Ludian earthquake. Seismol Geol 2015;37(1):279–90 (in Chinese).
[40] Liu C, Zheng Y, Xiong X, Fu R, Shan B, Diao F. Rupture process of Ms 6.5 Ludian earthquake constrained by regional broadband seismograms. Chin J Geophys 2014;57(9):3028–37.
[41] Lysmer J, Kuhlemeyer RL. Finite dynamic model for infinite media. J Eng Mech Div 1969;95(4):859–78.
[42] Somerville PG, Smith NF, Graves RW, Abrahamson NA. Modification of empirical strong ground motion attenuation relations to include the amplitude and duration effects of rupture directivity. Seismol Res Lett 1997;68:199–222.
[43] Kalkan E, Kunnath SK. Effects of fling step and forward directivity on seismic response of buildings. Earthq Spectra 2006;22(2):367–90.
[44] Wang M, Huang D, Wang G, Li D. An efficient framework for developing the data-driven Nemark displacement prediction model. J Geotech Geoenviron Eng 2020. accepted.
[45] Soga K, Alonso E, Yerro A, Kumar K, Bandara S. Trends in large-deformation analysis of landslide mass movements with particular emphasis on the material point method. Geotechnique 2016;66(3):248–73.
[46] Rathje EM. Seismic landslide assessments: bridging the gap between engineers and earth scientists. William B. Joyner Lecture, The 11th national conference on earthquake engineering, los angeles, June 25-29, 2018.